

Content type: Research

Shape and Size-Dependent Surface Plasmonic Resonances of Liquid Metal Alloy (EGaIn) Nanoparticles

Sina Jamalzadegan¹, Alireza Velayati¹, Mohammadreza Zare¹, Michael D. Dickey^{1}, and Qingshan Wei^{1*}*

¹Department of Chemical and Biomolecular Engineering, North Carolina State University, Raleigh, NC 27695, USA

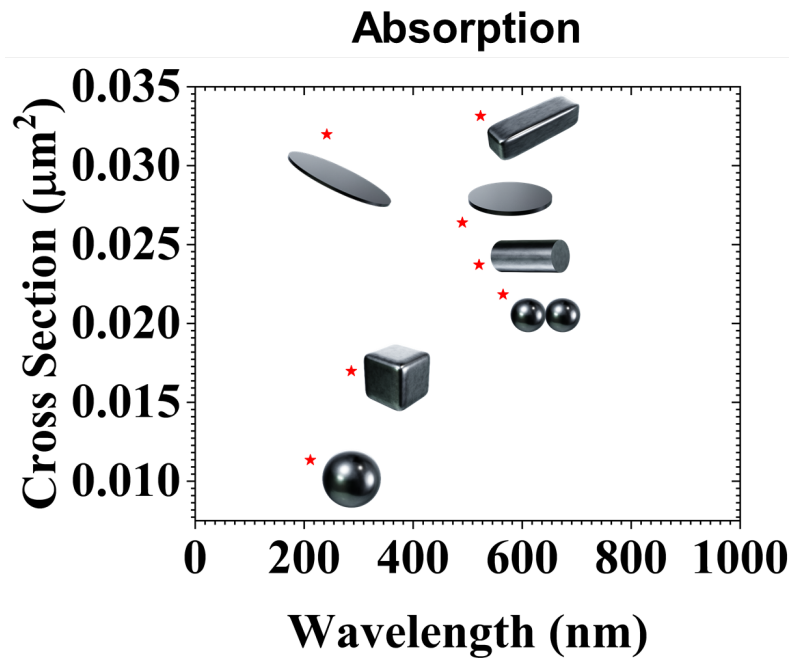
* Co-corresponding: qwei3@ncsu.edu and mddickey@ncsu.edu

Abstract

Liquid metals (LM) are emerging plasmonic nanomaterials with transformable surface plasmon resonances (SPR) due to their liquid-like deformability. This study delves into the plasmonic properties of LM nanoparticles, with a focus on EGaIn (eutectic gallium-indium)-based materials. Leveraging Finite-Difference Time-Domain (FDTD) simulations, we explored the localized SPR (LSPR) effects of EGaIn nanoparticles with various shapes, including nanospheres, dimers, nanorods, nanodisks, nanoellipses, nanocubes, and nanocuboids, in the broad range of ultraviolet (UV)-visible-near infrared (NIR) spectrum. EGaIn, known for its unique properties such as low toxicity, negligible vapor pressure, and excellent electrical and thermal conductivity, is appealing in broad wavelength plasmonic applications. In particular, this study reveals uncovered LSPR effects in the visible and NIR wavelength ranges, providing a comprehensive map of LSPR peaks and cross-sections for different shapes of EGaIn nanoparticles. The findings offer insights into correlating EGaIn nanoparticle geometry with their optical properties for diverse applications, ranging from biosensing, nanoelectronics, to optomechanical systems.

KEYWORDS: Liquid metal, EGaIn, surface plasmon resonance (SPR), FDTD, biosensor

Table of Contents



Introduction

With the rapid advancement of nanofabrication methods, nanoplasmonics has experienced significant growth and found applications in a wide range of research areas. The surface plasmon resonance (SPR) phenomenon occurs between a conductive material and a dielectric medium. Under conditions of resonance, the incident light induces the formation of a collective charge density wave that propagates along this interface, known as a surface plasmon polarization (SPP)¹⁻³. For metallic nanoparticles, the oscillation of electromagnetic waves is confined in close proximity to the nanoparticles themselves, resulting in an optical effect known as localized surface plasmon resonance (LSPR). The controlled manipulation of LSPR has given rise to a range of applications in areas such as biosensing^{1,4,5}, chemical detection⁶, 3D printing⁷, drug delivery⁸, and the development of wearable devices⁹. For sensing applications, the sensitivity of a SPR sensor is based on the ability to detect small changes in the refractive index surrounding the plasmonic surface that cause shifts in the SPR¹⁰. The SPR shifts can be carefully measured and correspond to the presence and concentration of target analytes. The significance of SPR in biosensing lies in its ability to enable real-time and label-free detection of biomolecules, which makes it a potent diagnostic tool¹¹.

Gold and silver are the two most commonly studied plasmonic nanomaterials, which exhibit tunable LSPR properties spanning from visible (vis) to near infrared (NIR) wavelength range¹². Alternative metals with LSPR features have also been reported. For instance, aluminum exhibits robust plasmon resonance across the ultraviolet (UV)-vis spectrum¹³. Platinum and palladium have been used for plasmonic optical gas sensing¹⁴. Copper could serve as plasmonic waveguides with exceptionally low losses, surpassing the performance of gold-based counterparts.¹⁵ However, most conventional plasmonic nanomaterials are rigid, meaning

mismatched mechanical properties when interfacing with biological surfaces. It also means fixed optical properties that cannot be flexibly modified based on the needs after synthesis or fabrication. On the other end, soft and stretchable plasmonic materials attract increased interests, because of the possibility of freely changing the shape, and thus, the SPR response of such materials. As such, soft and stretchable materials are finding various applications, ranging from soft robotics, e-skins, to stretchable electronics.

Gallium¹⁶⁻²⁰, indium^{17,21}, tin^{17,21}, magnesium²², bismuth^{23,24}, and their alloy compositions^{25,26} belong to the category of metals that exhibit plasmon resonance within the UV spectrum. Nanoparticles (NPs) fabricated from these materials may have different applications than gold and silver, which resonate in the visible range. For instance, plasmon-enhanced UV spectroscopy offers a valuable avenue to observe dynamic biochemical processes and characterize the chemical properties of these molecules in their native environment. As such, UV-plasmonic NPs find utility in various fields, such as biomedicine²⁷, label-free DNA analysis²⁸, single molecule sensing²⁹, and cardiovascular imaging³⁰⁻³².

Liquid metals (LMs) consisting of gallium and its alloys have recently attracted attention as a UV-plasmonic material^{16,18,21,33,34}. However, the UV region has not been the sole focus for LMs in recent years. Recent studies have highlighted the potential plasmonic properties of gallium alloy NPs in other wavelength regions, such as visible light and near-infrared (NIR)^{35,36}. Despite this, a thorough investigation into how shape and size affect the surface plasmonic resonances of gallium alloy NPs is still lacking.

Gallium possesses a melting point of 29.8 °C, which can be lowered below room temperature by combining it with other metals like indium and tin. This alloying process results in eutectic compositions with remarkably low melting points. One prominent example of such

eutectic composition is EGaIn (eutectic gallium-indium), consisting of 75 wt% gallium and 25 wt% indium, with a melting point of 15.7 °C. Furthermore, both gallium and EGaIn exhibit low toxicity, exhibit negligible vapor pressure at room temperature, have a viscosity approximately twice that of water, and possess excellent electrical and thermal conductivity³⁷⁻⁴³. Due to their low viscosity, EGaIn can be readily fragmented into colloidal droplets through various techniques⁴⁴. Recent reviews have extensively examined the utilization of these droplets, including their applications in sensors, microfluidic systems, robotics, electronic circuits, catalysis, energy harvesting, and even biomedical applications like drug delivery⁴⁴⁻⁴⁶. Currently, the prevalent methods for generating LMNPs (liquid metal nanoparticles) are primarily based on employing microfluidic, sonication, and shearing processes⁴⁵.

Gallium exhibits a Drude-like dielectric permittivity profile that spans from the UV range⁴⁷ all the way into the NIR region^{25,33}. Moreover, within nanoscale constraints, the oscillations of charge carriers can be readily affected by slight alterations in size, geometry, material composition, and variations in the surrounding dielectric environment in which the nanoparticles are embedded. Recent computational studies examined the LSPR sensitivity of rod-shaped core-shell GaAg, GaAl, GaHg, and Ga (85.8%) In (14.2%) (which is not EGaIn) NPs. These studies showed a red shift of the extinction spectrum peaks of GaAg from the UV to the visible light range by varying the aspect ratio and shell thickness. In contrast, Ga NPs alone exhibited dominant peaks in scattering and absorption power cross-section spectra in the UV wavelength range. Additionally, Ga (85.8%) In (14.2%) NPs did not show a substantial LSPR effect compared to GaAg⁴⁸⁻⁵⁰. Although these computational studies focused on gallium alloys, they still lack computational findings on EGaIn surface plasmon resonance features. In the limited examples in the past, the UV plasmonic features of 100 nm diameter EGaIn NPs have been experimentally and computationally

confirmed⁵¹. Nevertheless, a thorough study on the correlation of the LM shape and size with their LSPR properties has not been presented.

Gallium and its liquid alloys are appealing due to the possibility of shape-transformation and constructing reconfigurable plasmonic devices. Thus, it is critical to substantiate theoretical projections related to gallium nanoparticles concerning their dimensions, geometry, response to the surrounding dielectric environment, and their integration with other plasmonic materials, leading to the controllable optical and plasmonic characteristics. Furthermore, with improvements in the fabrication^{52,53} and synthesis of liquid metal nanodroplets with distinct shapes, it is imperative to explore how the various nanoparticle geometries influence the manifestation of their unique properties. We focus on EGaIn as a representative LM to illustrate how “liquid plasmonics” can be rationally programmed by controlling the size and shape. By combining its robust SPR properties, geometry-tailored plasmonic effects, and outstanding non-optical properties, EGaIn nanoplasmonics offers exciting opportunities for applications in photoacoustics, nanoelectronics, nanoscale electrochemistry⁵⁴, and optomechanical systems⁵⁵.

In this study, we applied Finite-Difference Time-Domain (FDTD) numerical simulation technique⁵⁶ to investigate the geometry-LSPR relationship of EGaIn-based LM nanomaterials. FDTD is a computational tool frequently used to study electromagnetic wave propagation, reflection, and scattering in complex geometries and materials. We investigated the scattering and absorption cross-section spectra of EGaIn NPs with different shapes and sizes, as well as their coupling with gold and silver NPs, to identify characteristic plasmon-resonant peaks in the wide UV-vis-NIR range. The results can be used to guide the future synthesis of EGaIn NPs with desired optical properties that are useful for various optical biosensing applications.

Method

The FDTD numerical simulation was run by the Ansys Lumerical software (2022 R2.1). The permittivity of EGaIn in the 400–1000 nm range reported in the literature²⁵ was extrapolated to the UV range of 100–400 nm using the Drude-Lorentz equations (**Equations 1 and 2**):

$$\varepsilon_1(E) = 1 - \frac{E_p^2}{(E^2 + \gamma^2)} \quad (1)$$

$$\varepsilon_2(E) = 1 - \frac{E_p^2\gamma}{E(E^2 + \gamma^2)} \quad (2)$$

where ε_1 and ε_2 represent the real and imaginary part of the permittivity, respectively. E_p and γ represent the plasma frequency and broadening parameters. These two parameters were calculated by fitting the experimental refractive index data²⁵ using the Drude-Lorentz model. **Figure S1** shows the extrapolated and experimental real and imaginary parts of the permittivity of EGaIn in the 100–1000 nm wavelength range. The simulation time was set to 1000 fs at 300 K, and the refractive index of the surrounding medium was set to 1, which corresponds to air. The model ignores any surface oxides or adsorbate molecules. The mesh size was set uniformly at 0.5 nm. A s-polarized (90° polarization angle) plane source with 100–1000 nm wavelength was used to study the absorption and scattering power cross-section responses. **Figure S2** schematically shows the FDTD simulation setup with the incident light source and polarization angle.

Results

SPR effects of 0D EGaIn nanoparticles

EGaIn Nanospheres. A nanosphere is a zero-dimensional (0D) nanoparticle characterized by its spherical shape. Nanospheres have uniform diameters that typically range from a few nanometers to hundreds of nanometers. Their properties and behaviors often differ from those of

bulk materials due to quantum effects and size-related phenomena. Studying LM nanospheres is sensible because liquids naturally like to assume spherical shapes due to surface tension.

As an initial step, we examined the scattering and absorption cross-sections of individual spherical EGaIn nanoparticles with varying diameters ranging from 20 to 200 nm (**Figure 1**). Power cross-section is the probability of light energy being absorbed or scattered by the objects, which is the key parameter for assessing how effectively a material interacts with light, quantifying its energy absorption and scattering capabilities across wavelengths. Our study utilizes absorption and scattering power cross-sections across UV to near-IR wavelengths for characterizing various shapes and sizes of EGaIn nanoparticles (**Figure 1a**). Using Lumerical Ansys software, we extracted the computed electric field data for a 200-nm single spherical EGaIn particle at a 253 nm wavelength (major scattering peak) and plotted the electric field heat map using Python packages (**Figure 1b**). For the smaller sizes of EGaIn nanoparticles (20-100 nm), the absorption cross-section spectra exhibit SPR effects mainly within the UV range (around 200 nm wavelength) (**Figure 1c**). The amplitude of the dominant LSPR in the absorption spectra increases with the increase of LM NP size, a phenomenon that was corroborated by a recent simulation study⁵¹. In addition, the absorption spectrum of a 100 nm spherical EGaIn nanoparticle displays dominant peaks within the UV range (**Figure 1c**), consistent with prior experiments and simulation model⁵¹. Furthermore, the FDTD simulation results indicate that as the NP size increases, a secondary LSPR peak becomes more and more evident within the visible light spectrum (400-700 nm) and the near-infrared (IR) range (700-1000 nm) of the absorption spectra (**Figure 1c**). The visible SPR response of spherical EGaIn nanoparticles is even more obvious in the scattering spectra (**Figure 1d**). This observation indicates EGaIn NPs could be excellent scattering contrast agents in the visible wavelength range.

To validate our FDTD findings, we also simulated the absorption and scattering cross-section spectra with Mie theory⁵⁷ and compared with FDTD results. The formulas presented in **Equations 3 and 4** represent the scattering and absorption cross-sections (σ) derived from the Mie theory, where a is the radius of a spherical nanoparticle and $\alpha = \frac{2\pi a}{\lambda}$. Also, a_n and b_n are the Mie theory coefficients, which represent the magnetic and electric poles of order n , respectively. The cross-section spectra obtained using Mie theory exhibit a close correspondence with the FDTD results (**Figure S3**). LMs are known to have an ultrathin (~ 3 nm) oxide layer, which is naturally formed under ambient conditions. We also studied the effects of the oxide layer on the LSPR properties of EGaIn NPs. We ran a simulation of a 200-nm spherical EGaIn NP with a 6-nm oxide layer. The FDTD simulation results showed that the thin oxide layer did not impact the plasmonic features of the EGaIn NP, as no obvious changes were observed in the absorption and scattering spectra compared to the pure EGaIn NPs without the oxide layer (**Figure S4**). Furthermore, we explored the SPR effects of single gallium (Ga) spherical NPs (**Figure S5**). Similar to the single EGaIn NPs, we observed that the LSPR of the single Ga NPs shows a prominent peak in the UV range in both the absorption and scattering cross-section spectra. Like EGaIn NPs, the scattering cross-section spectra of Ga NPs also have a secondary peak within the visible light range and its position redshifts as the particle size increases. It is worth mentioning that compared to EGaIn, gallium has a melting point slightly above room temperature. Yet, it is typically found as a liquid at room temperature due to its ability to supercool⁵⁸. The supercooling is thought to arise, in part, because of the oxide layer and also the effect of using particles to limit heterogeneous nucleation.

$$\sigma_{absorption} = \frac{\pi a^2}{\alpha^2} \left| \sum_{n=1}^{\infty} (2n+1)(-1)^n (a_n - b_n) \right|^2 \quad (3)$$

$$\sigma_{scattering} = \frac{2\pi a^2}{\alpha^2} \sum_{n=1}^{\infty} (2n+1) (|a_n|^2 + |b_n|^2) \quad (4)$$

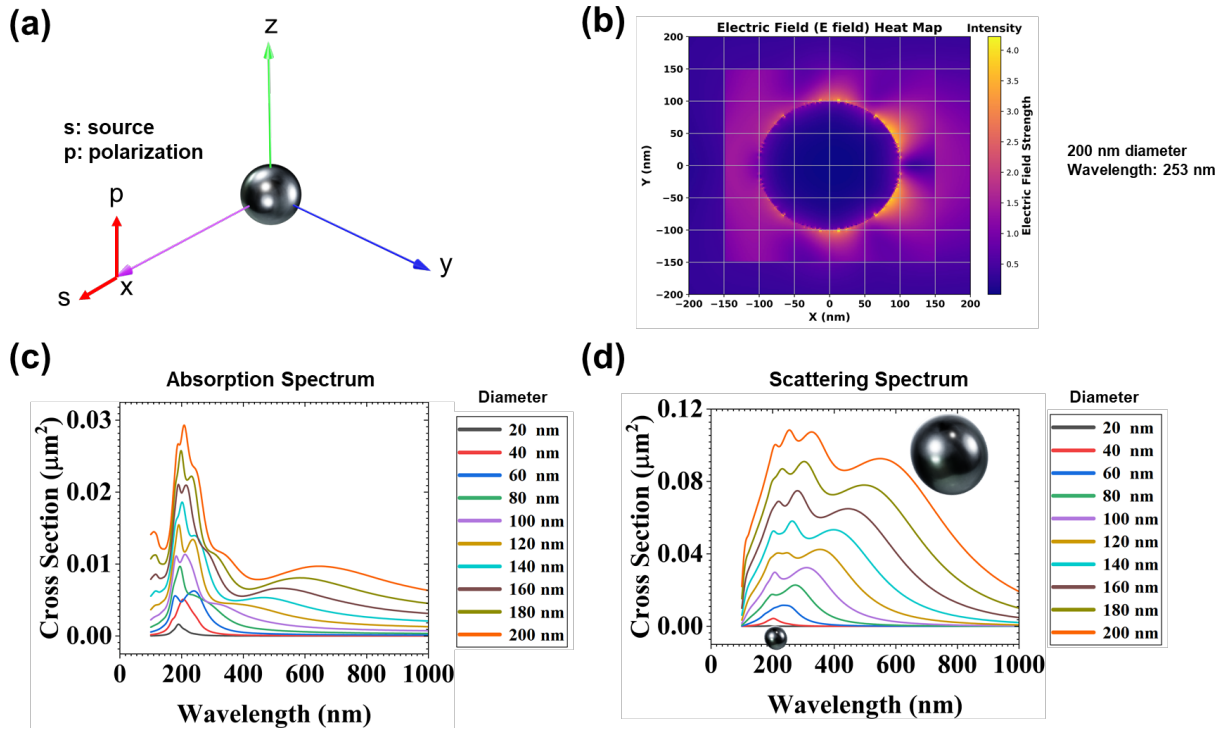


Figure 1. Plasmonic resonance behavior of a single spherical EGaIn nanoparticle. a) 3D schematic of a single spherical EGaIn NP excited by a plane-wave light source (s) with 90° polarized angle (p). b) Electrical field (E field) heat map for a 200-nm diameter spherical EGaIn nanoparticle excited at 253-nm wavelength (corresponding to its major scattering peak). The plane-wave light source propagates in x-direction from left to right. c) Absorption and d) scattering cross-section spectra of single spherical EGaIn nanoparticles with various diameters (20-200 nm).

EGaIn Nanocubes. Nano-sized cubic-shaped NPs exhibit unique properties owing to their well-defined structures and sharp corners. These properties include a high surface area-to-volume ratio, making them excellent candidates for catalytic applications, as well as efficient drug delivery carriers due to their enhanced surface reactivity. Their distinct geometry leads to plasmonic enhancement (e.g., hot spots), enabling applications in sensing and imaging. Additionally, the

crystalline nature of cubic nanoparticles ensures remarkable stability and controlled surface chemistry, facilitating precise tuning of their electronic, optical, and magnetic characteristics. These properties make nano-sized cubic-shaped nanoparticles invaluable in a wide range of fields. While fabricating EGaIn NPs with cubic shapes poses a significant challenge due to the high surface tension of EGaIn, our study focused on investigating the SPR effects of these NPs for potential future research endeavors in this field.

Figure 2 displays the absorption and scattering power cross-section spectra for cubic EGaIn NPs ranging from 50 to 400 nm in cubic size. Using Lumerical Ansys software, we extracted the electric field data for a 400-nm single EGaIn nanocube at 215 nm and 970 nm wavelengths (major scattering peaks), respectively, and plotted the electric field heat maps of both using Python packages (**Figure 2b**). The 2D field maps showed enhanced LSPR effects (or hot spots) either at the edges or corners of nanocubes, depending on the excitation wavelengths. The absorption power cross-section spectrum reveals the presence of two plasmon resonance response regions: one in the UV range (mode I, around 200 nm), characteristic of EGaIn, and the other one in the vis-NIR range (mode II), which is observed for nanocubes larger than 100 nm size (**Figure 2c**). The mode I peak also consists of several small peaks. Notably, as the size of the cubic-shaped EGaIn nanoparticles increases, resonant mode I of nanocubes remains at around 200 nm, while mode II peaks exhibit a redshift all the way into the NIR region with increased peak intensity (**Figure 2c**). The scattering power cross-section spectra also demonstrated two major peaks in the UV and vis-NIR regions, respectively. However, the latter has a much higher amplitude than the UV resonant mode, indicating EGaIn nanocubes are better scatterers in the vis-NIR region compared with UV wavelengths (**Figure 2d**).

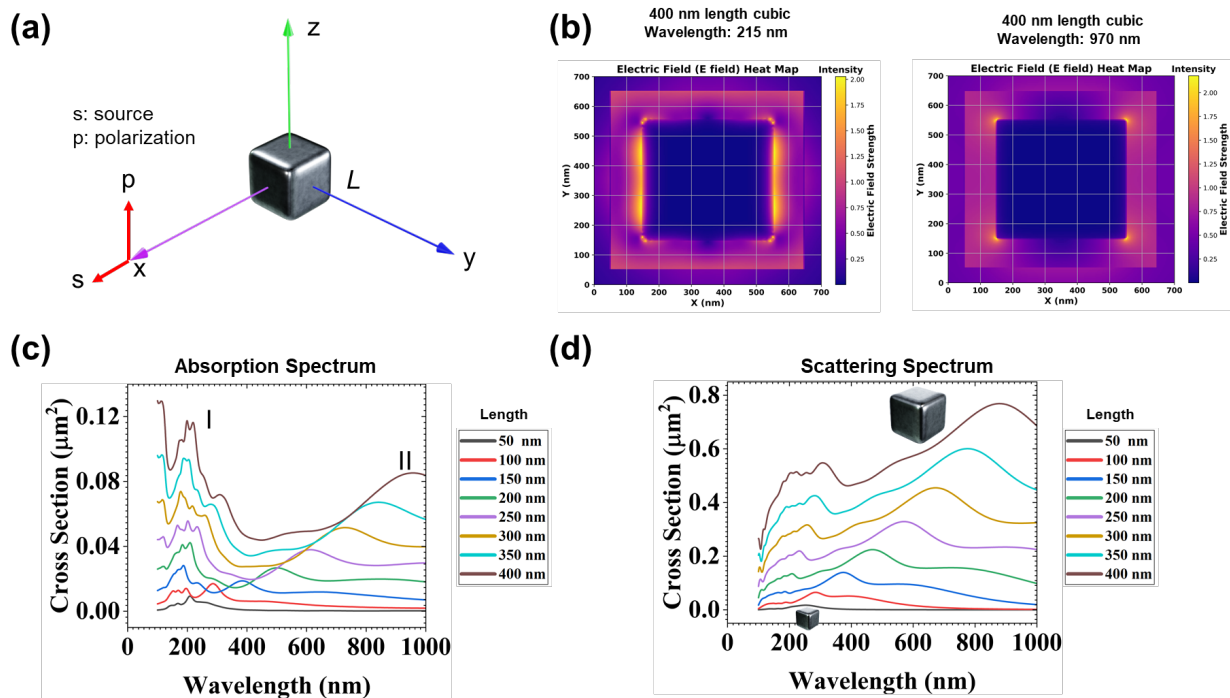


Figure 2. Plasmonic resonance behavior of single cubic EGaIn nanoparticle. a) 3D schematic of single cubic EGaIn nanoparticle excited by a plane-wave light source (s) in x-direction with a 90 degree polarization (p) angle. b) Electrical field (E field) heat map for a 400-nm length cubic EGaIn nanoparticle excited at 215 nm and 970 nm wavelength (major absorption peaks), respectively. The plane-wave light source propagates in x-direction from left to right. c) Absorption and d) scattering cross-section spectrums of EGaIn nanocubes with various lengths (50-400 nm).

SPR effects of 1D EGaIn nanoparticles

EGaIn Nanorods. Here, a cylinder is chosen as a simple model for FDTD simulation of 1D LM materials. Nanorods may refer to any low aspect ratio (AR) 1D nanomaterials with many other noncircular cross-section shapes, such as square or pentagon. When the AR exceeds 10-20, these 1D nanomaterials are also generally referred to as nanowires. EGaIn nanorods, measuring

210 nm in diameter and 850 nm in length, were previously synthesized via an ultrasound-assisted physical dispersion technique⁵⁹. In a different method, EGaIn droplets anchored to a flat substrate were pulled perpendicular to the substrate surface at room temperature, resulting in the formation of an hourglass shaped EGaIn structure. Subsequent pulling leads to the breakdown of this bridge, ultimately resulting in the formation of EGaIn NWs on the surface at the point of rupture⁶⁰. Thus, different from the nanocubes, 1D LM materials have already been realistically prepared.

We investigated the surface plasmon resonance of single EGaIn nanorods by altering both the diameter and length of individual EGaIn nanorods. **Figure 3a** illustrates the schematic representation of a single EGaIn nanorod, with a constant diameter (20 nm) while varying its length (20-1000 nm). **Figures 3a, d, and g** display the exposure of a single EGaIn nanorod to a polarized plane-wave source in all three directions. The results of the absorption (**Figures 3e and 3h**) and scattering (**Figures 3f and 3i**) cross-sections for both the y and z plane-wave sources revealed two prominent peaks in the UV range. Additionally, as the length of the nanorods increased, the LSPR peaks of both scattering and absorption cross-section spectra also increased. Notably, when switching to an x-direction plane-wave source, we observed a dominant LSPR peak shifted into the visible light range for both absorption (**Figure 3b**) and scattering (**Figure 3c**) cross-section spectra, while a weak LSPR peak remained in the short wavelength range (<400 nm). We attribute the short wavelength LSPR responses to the transverse mode of the LM nanorod, which is by large independent of the AR of nanorods, while the visible LSPR peaks to the longitudinal mode of the nanorod, which redshifts significantly as the increase of AR.

By maintaining a constant length (1000 nm) while varying the diameter of these nanorods, we observed SPR effects mainly confined in the UV range (**Figure S6**). As anticipated, both the

scattering and absorption cross-sections increased with an increase in the radius of these nanorods (Figure S6).

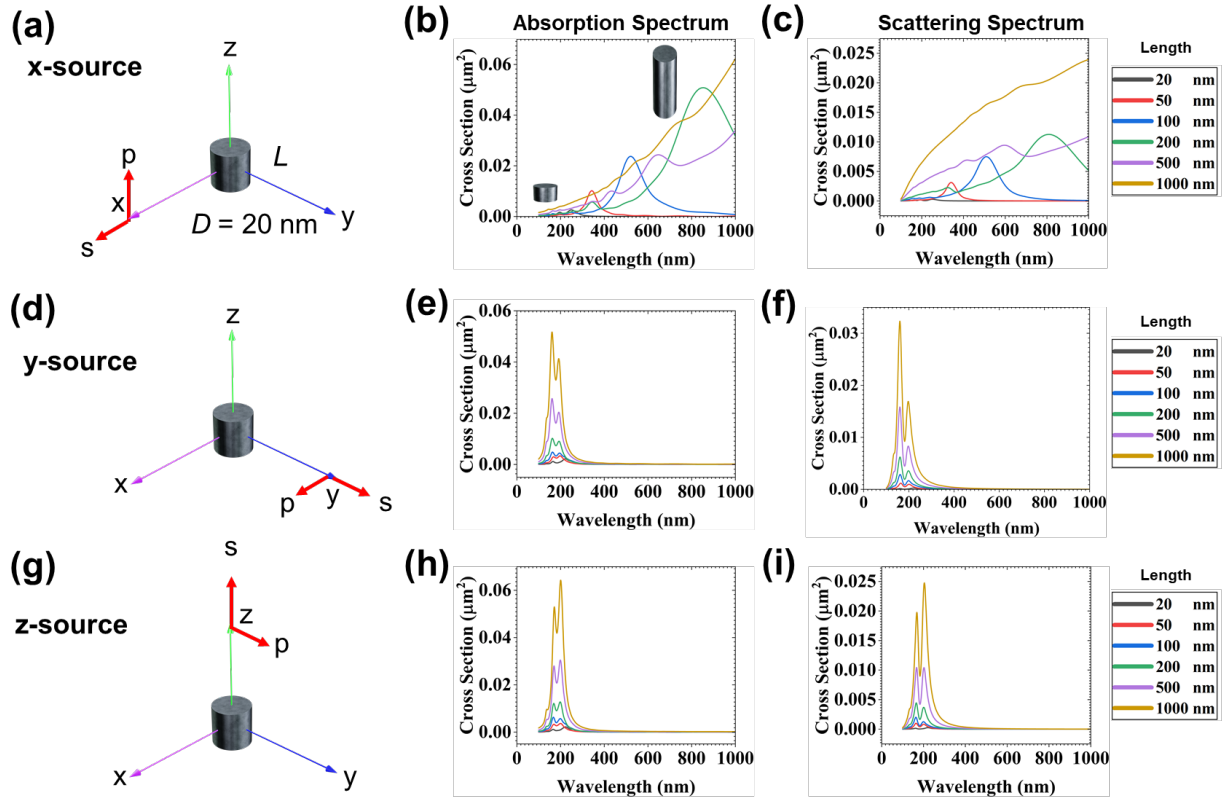


Figure 3. Plasmonic resonance behavior of single EGaIn nanorod. a,d,g) 3D schematic of single EGaIn nanorod excited by a plane-wave light source (s) in x-, y-, and z-directions with 90 degree polarization (p), respectively. b,e,h) Absorption and c,f,i) scattering cross-section spectra for various lengths with a constant diameter of 20 nm.

EGaIn Nanocuboids. Nanocuboid is another type of 1D EGaIn, which has a square cross-section and tunable length. Such a structure has not been fabricated yet for EGaIn. To investigate the LSPR effects of EGaIn nanocuboids, we simulated the absorption and scattering power cross-section spectra using plane-wave sources in all three directions for single EGaIn nanocuboids with a $100 \times 100 \text{ nm}$ cross-section and various lengths from 5 to 500 nm (Figure 4). For the absorption

(Figure 4b) and scattering (Figure 4c) spectra of the single EGeIn nanocuboid excited by a plane-wave light source in the x-direction (Figure 4a), a multi-mode LSPR response was observed, with the major LSPR peak located in the vis-NIR wavelength range. Similar to the LM nanorods, this dominant peak is attributed to the longitudinal resonance of the nanocuboids.

For y and z-direction excitation (Figures 4d and 4g), the major peaks of the absorption (Figures 4e and 4h) and scattering spectra (Figures 4f and 4i) showed a blue-shift into the UV range as the cuboid length increases. For the absorption (Figure 4e) spectra of the single EGeIn nanocuboid excited by a plane-wave light source in the y-direction (Figure 4d), the UV LSPR peak also split into two for lengths larger than 20 nm. We attributed the multi-mode LSPR responses of nanocuboids to the strong edge effects due to the geometry. More detailed simulation studies are required to understand the origine of these peaks further.

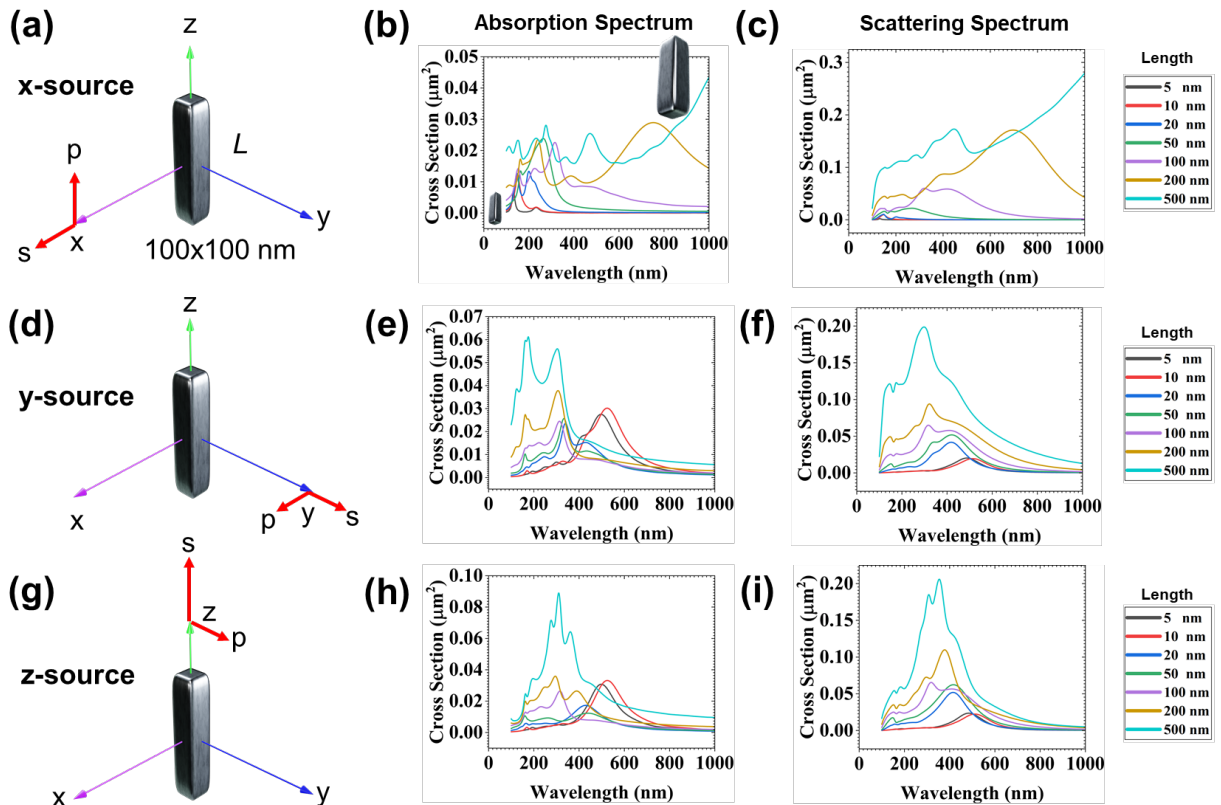


Figure 4. Plasmonic resonance behavior of single EGaIn nanocuboid. a,d,g) 3D schematic of a single EGaIn nanocuboid excited by a plane-wave light source (s) in x-, y-, and z-direction with 90 degree polarization (p), respectively. b,e,h) Absorption and c,f,i) scattering cross-section spectra for various lengths with constant cross-section area of 100x100 nm.

SPR effects of 2D EGaIn nanoparticles

EGaIn Nanodisks. 2D EGaIn nanostructures include several shapes, such as nanodisks and nanoellipses. Nanodisks are disk-like structures with two flat surfaces. **Figure 5** illustrates the absorption and scattering cross-sections of a single EGaIn nanodisk (5 nm thick) under the excitation of three distinct plane-wave source directions. When utilizing an x-direction plane-wave source, both the absorption (**Figure 5b**) and scattering (**Figure 5c**) cross-section spectra exhibited a single SPR peak of EGaIn nanodisks in the UV range. As the diameter of EGaIn nanodisk increased, the peak experienced a slight redshift, accompanied by an dramatic increase in the power of cross-sections. When employing a y-direction plane-wave source, the previous UV LSPR peaks disappeared (**Figures 5e and 5f**). Instead, for larger nanodisks, such as 100 nm and 200 nm diameter nanodisks, broad SPR peaks appeared in the visible and NIR wavelength ranges for both absorption (**Figure 5e**) and scattering (**Figure 5f**) spectra. The intensity of such peaks increased with the increase of nanodisk diameter. In a similar manner, the z-direction plane-wave source produced a prominent SPR peak in the visible and NIR regions for both absorption (**Figure 5h**) and scattering (**Figure 5i**) spectra. These results suggested that EGaIn nanodisks could be very active NIR-responsive plasmonic materials under right excitation.

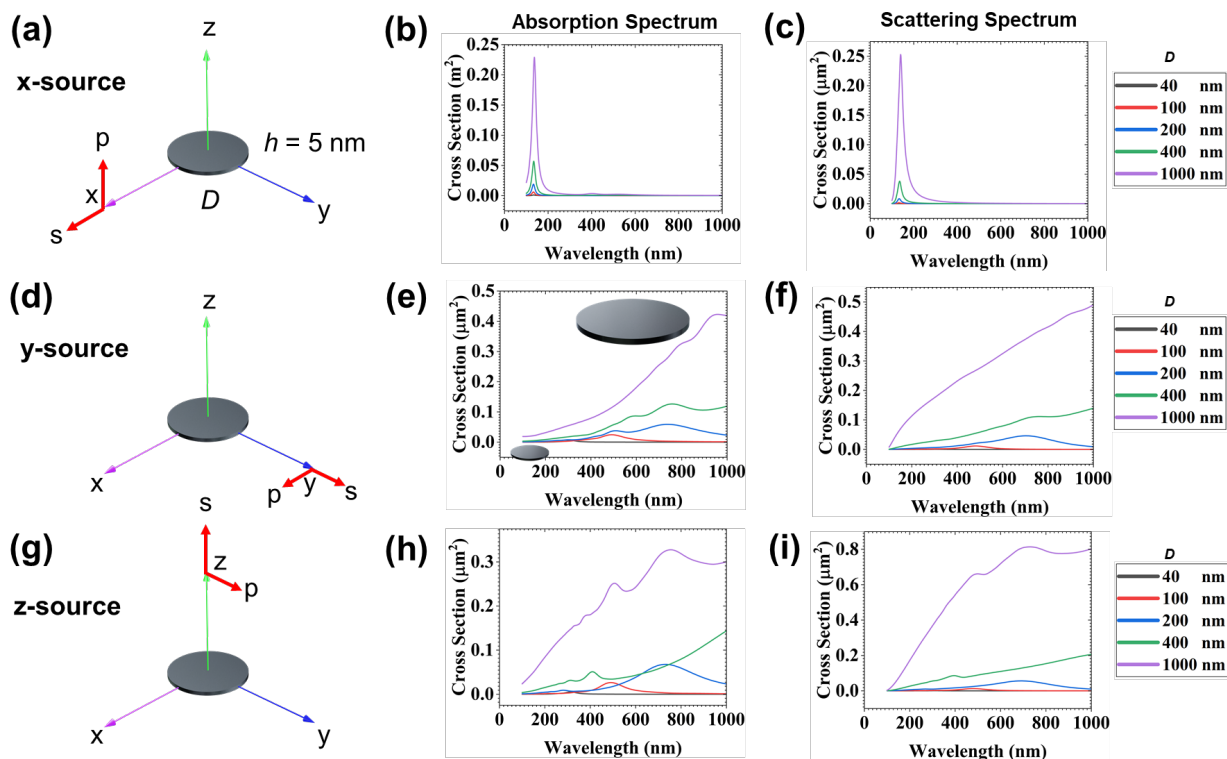


Figure 5. Plasmonic resonance behavior of single EGaIn nanodisk. a,d,g) 3D schematic of single EGaIn nanodisk excited by a plane-wave light source (s) in x-, y-, and z-directions with 90 degree polarization (p), respectively. b,e,h) Absorption and c,f,i) scattering cross-section spectrums for various diameters with fixed 5 nm thickness.

EGaIn Nanoellipses. Nanoellipses are 2D structures with two asymmetric axes (a and b). Previously, laser ablation of gallium metal was utilized to synthesize ellipse-like GaOOH particles in an aqueous solution. The successful formation of well-defined GaOOH structures was controlled by the addition of cationic CTAB surfactant⁶¹. Fabrication of EGaIn nanoellipses has not been demonstrated before. However, it is essential to study the LSPR of EGaIn nanoellipsoids to explore their unknown optical properties and corresponding applications in various fields. We investigated the LSPR effects of single EGaIn nanoellipses by fixing the thickness (50 nm) and

the length of minor axis ($b=100$ nm, **Figure S7**). **Figure S7** presents the absorption and scattering cross-section spectra of this NP shape. By applying a plane-wave source in the x-direction (**Figure S7a**), we observed LSPR effects of EGaIn nanoellipses mainly in the UV range for ellipsoids with varied major axis, ranging from 100 to 1000 nm, while keeping the minor axis constant at 100 nm (**Figure S7b and S7c**). While the dominant peaks are located at ~ 300 nm, there is a notable shoulder peak at ~ 150 nm in the deep UV range. Additionally, the power cross-section for both absorption and scattering spectra increased with the increase of the ellipse's major axis. When applying a plane-wave source in the z-direction (**Figure S7g**), we observed a similar plasmon resonance behavior in the UV range (**Figure S7h and S7i**). Interestingly, when applying a plane-wave source in the y-direction (**Figure S7d**), we observed multimodal LSPR responses of single EGaIn nanoellipses with radius sizes of long axis in the broad spectra of visible and NIR wavelengths (**Figure S7e and S7f**). The longer the major axis, the more LSPR modes the nanoellipses have. We attributed the increasing number of resonant modes to the transition of oval shapes of nanoellipses into 1D geometries when the ratio of major to minor axis increases.

Plasmonic Coupling of EGaIn NPs

EGaIn-EGaIn coupling. In addition to particle size and shape, the distance of neighboring plasmonic NPs will also affect its own LSPR property due to SPR overlapping, an effect also known as plasmonic coupling. The plasmonic coupling effect of noble metals such as gold⁶² and silver⁶³ has been well studied previously by employing spherical nanoparticle dimers as models. In a similar vein, here we investigated the SPR coupling effects of spherical dimer NPs made of EGaIn. In the FDTD simulation, we constructed EGaIn dimers with different particle sizes (**Figure**

6). Using Lumerical Ansys software, we extracted the computed electric field data for a 100-nm dimer spherical EGaIn particles excited by a 210 nm wavelength plane-wave in all directions with 90 degree polarization and plotted the electric field heat map using Python packages (**Figure 6b, 6f, and 6j**). The results showed that by changing the orientation of the excitation source, it is possible to control the hot spot locations, either in between or at the outside edge of the dimers. The whole spectra results indicate that when employing a plane-wave source oriented along the x (**Figures 6c, and 6d**) and z (**Figures 6g and 6h**) directions, mild plasmonic coupling occurred for the dimers with a new SPR peak appearing at around 200-300 nm. Moreover, these peaks exhibited a redshift as the dimer size increased. Notably, when the plane-wave source was oriented along the y direction, the coupling effect was more significant, with a dominant coupling peak emerging within the visible light and NIR spectrum (**Figures 6g and 6h**). Again, a larger dimer size correlates with redshifted and enhanced resonance-coupled peaks.

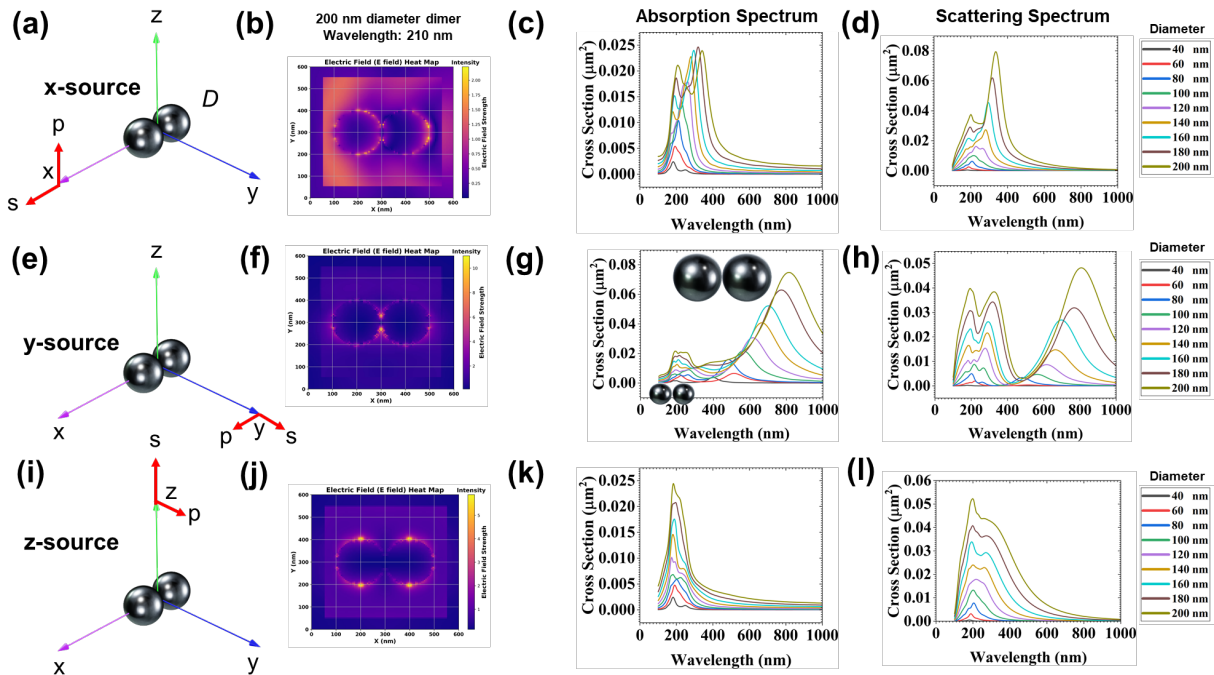


Figure 6. Plasmonic resonance behavior of spherical EGaIn dimers. a, e, i) 3D schematic of spherical EGaIn dimers excited by a plane-wave light source (s) in x-, y-, and z-direction with 90 degree polarization (p), respectively. b, f, j) Electrical field (E field) heat map for 100 nm diameter spherical EGaIn nanoparticle dimer at 210 nm wavelength excited by a plane-wave light source (s) in x-,y-, and z-direction with 90 degree polarization (p), respectively. c, g, k) Absorption and d, h, l) scattering cross-section spectra for EGaIn dimers with various individual particle sizes.

EGaIn-Au and EGaIn-Ag coupling. Additionally, we investigated the LSPR coupling behavior of EGaIn-noble metal dimers, such as EGaIn-Au and EGaIn-Ag dimers. **Figures S8** illustrates the absorption and scattering cross-section spectra for EGaIn-Au and EGaIn-Ag dimers, encompassing various dimer sizes ranging from 80 to 200 nm. When compared to single EGaIn nanospheres, which exhibit characteristics SPR in the UV range (ca. 200 nm), and single silver and gold spherical nanoparticles, which display SPR in the 400 and 500 nm range, the EGaIn-Au and EGaIn-Ag dimers exhibit prominent redshifted resonant peaks within the visible light range. The coupling-induced redshift is also strongly proportional to the size of dimers. Such strong coupling effect between soft EGaIn and rigid noble metal nanoparticles may open new applications in biosensing.

Discussion

The aim of this study is to conduct a comprehensive investigation of the LSPR effects of EGaIn NPs by simulating the absorption and scattering power cross-section spectra for various shapes. A summary of all simulation results is presented in **Figure 7**, which illustrates a roadmap for the locations of major LSPR peaks of various EGaIn NPs, which have at least one dimension

smaller than 100 nm. This map could be a quick guide for the researchers to determine the best shape of EGaIn NPs to achieve desired optical properties and therefore the optimal applications in various fields such as optical biosensors, medical bio-imaging, and drug delivery. For instance, for UV plasmonic applications, researchers may choose EGaIn nanospheres or nanoellipses for higher absorption efficiency. Similarly, for scattering contrast agents in the visible range, EGaIn nanorods seem a promising candidate due to balanced wavelength coverage and cross-section intensity. Overall, these major peaks in both scattering and absorption power cross-section spectra indicate that different shapes of EGaIn nanoparticles from 0D to 2D exhibit active SPR responses not only in the UV wavelength range, but also across visible to NIR wavelength regions. This is the first systematic study, demonstrating the unique optical activities of shape-controlled EGaIn NPs within the broad visible and NIR ranges. The SPR map can be used to guide the fabrication of various shapes of EGaIn nanoparticles to utilize their SPR advantages.

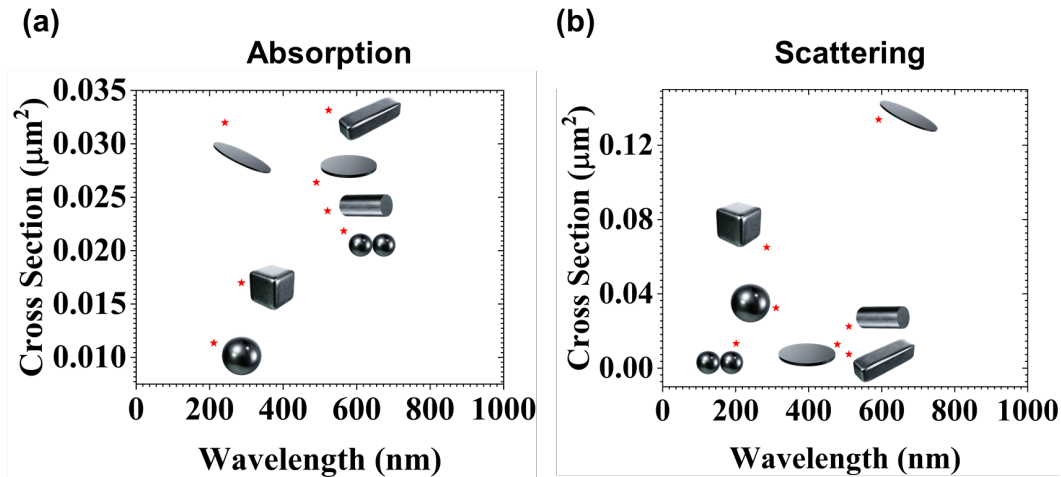


Figure 7. A guide map of transformable EGaIn nanoplasmonics. Peak absorption (a) and scattering (b) wavelengths and corresponding cross-sections for different shapes that have been simulated by FDTD.

To date, various shapes of LM NPs have been successfully fabricated using different techniques. For instance, EGaIn spherical NPs were synthesized through sonication⁵¹. EGaIn nanorods, measuring 210 nm in diameter and 850 nm in length, were created using ultrasound-assisted physical dispersion⁵⁹. Arrays of EGaIn nanowires were formed by pulling an EGaIn droplet on a flat substrate at room temperature, resulting in an hourglass-shaped structure that evolved into nanowires through a breakdown process⁶⁰. EGaIn nanodroplets were synthesized through polymeric ligand encapsulation, involving the covalent bonding of various polymers⁶⁴. Additionally, a recent nanofabrication technique took advantage of intermetallic wetting between Au and EGaIn LM on a Si/SiO₂ substrate, yielding LM nanostructures of different 2D geometries such as square, circle, and hexagonal disk shapes⁶⁵. The fabricated LM nanostructures exhibited smooth thin-film surfaces, sharp edges, and corners, with lateral feature sizes down to ~500 nm and the smallest spacing between array elements demonstrated to date (~250 nm). The LM nanostructures showed strong resonant optical responses in the broad UV-vis-NIR region, as indicated by the FDTD results (**Figure 7**). Such rich SPR properties will also promote the development of new fabrication technologies to generate shapes that have not been fabricated before. In particular, technology that can transform the shape of EGaIn nanoparticles is even more interesting, as that achieves the ultimate goal of transformable plasmonics. Integrating the new fabrication techniques and experimental measurements with FDTD simulation to confirm the SPR properties of EGaIn NPs could be one of future directions. The collaborative results will further convince LM's emerging applications in biosensing and many others^{66,67}.

Conclusion

To summarize, this study provides a comprehensive exploration of shape and size-dependent LSPR properties of EGaIn NPs in the broad UV-vis-NIR spectral range. Through FDTD simulations, we have investigated the LSPR effects exhibited by EGaIn nanoparticles across various shapes, including 0D, 1D, 2D, and plasmonic coupling formed by nanosphere dimers. The size-dependent SPR effects observed in the UV, visible, and NIR light ranges highlight the significance of tailored nanoparticle geometry in achieving desired optical and plasmonic characteristics. The presented guide map of major peaks and absorption and scattering power cross-sections for different shapes of EGaIn nanoparticles (Figure 7) serves as a valuable resource for researchers seeking optimal configurations for specific applications, including biosensing, medical bio-imaging, drug delivery, and beyond. This research not only contributes to the fundamental understanding of EGaIn NP behavior but also underscores the potential for shape-transformable gallium-based nanoparticles. As the field of “liquid plasmonics” continues to evolve, the findings presented here pave the way for further advancements in nanofabrication techniques and the development of novel applications in diverse scientific and technological domains.

Author contributions

Project conception and visualization were performed by SJ, MD, and QW. FDTD computational simulation and Mie theory computational study were conducted by SJ. Data analysis was performed by SJ. AV designed 3D schematic shapes of EGaIn with Blender. MZ assisted with the introduction section of the manuscript. SJ, MD, and QW wrote the manuscript. All authors contributed to the revision of the manuscript.

Acknowledgements

The authors sincerely thank the funding support from the National Science Foundation (Award # 1944167).

Conflict of Interest

The authors declare no competing financial interests.

References

- (1) Han, X.; Liu, K.; Sun, C. Plasmonics for Biosensing. *Materials* **2019**, *12* (9), 1411. <https://doi.org/10.3390/ma12091411>.
- (2) Maier, S. *Plasmonics: Fundamentals and Applications*; 2007. <https://doi.org/10.1007/0-387-37825-1>.
- (3) Kelly, K. L.; Coronado, E.; Zhao, L. L.; Schatz, G. C. The Optical Properties of Metal Nanoparticles: The Influence of Size, Shape, and Dielectric Environment. *J. Phys. Chem. B* **2003**, *107* (3), 668–677. <https://doi.org/10.1021/jp026731y>.
- (4) Guo, L.; Xu, S.; Ma, X.; Qiu, B.; Lin, Z.; Chen, G. Dual-Color Plasmonic Enzyme-Linked Immunosorbent Assay Based on Enzyme-Mediated Etching of Au Nanoparticles. *Sci. Rep.* **2016**, *6* (1), 32755. <https://doi.org/10.1038/srep32755>.
- (5) Im, H.; Shao, H.; Park, Y. I.; Peterson, V. M.; Castro, C. M.; Weissleder, R.; Lee, H. Label-Free Detection and Molecular Profiling of Exosomes with a Nano-Plasmonic Sensor. *Nat. Biotechnol.* **2014**, *32* (5), 490–495. <https://doi.org/10.1038/nbt.2886>.
- (6) Wang, S.; Forzani, E. S.; Tao, N. Detection of Heavy Metal Ions in Water by High-Resolution Surface Plasmon Resonance Spectroscopy Combined with Anodic Stripping Voltammetry. *Anal. Chem.* **2007**, *79* (12), 4427–4432. <https://doi.org/10.1021/ac0621773>.
- (7) Zou, Z.; Chen, Y.; Yuan, S.; Luo, N.; Li, J.; He, Y. 3D Printing of Liquid Metals: Recent Advancements and Challenges. *Adv. Funct. Mater.* **2023**, *33* (10), 2213312. <https://doi.org/10.1002/adfm.202213312>.
- (8) Kurzątkowska, K.; Santiago, T.; Hepel, M. Plasmonic Nanocarrier Grid-Enhanced Raman Sensor for Studies of Anticancer Drug Delivery. *Biosens. Bioelectron.* **2017**, *91*, 780–787. <https://doi.org/10.1016/j.bios.2017.01.049>.
- (9) *Surface Modification of Gallium-Based Liquid Metals: Mechanisms and Applications in Biomedical Sensors and Soft Actuators - Kwon - 2021 - Advanced Intelligent Systems - Wiley Online Library*. <https://onlinelibrary.wiley.com/doi/full/10.1002/aisy.202000159> (accessed 2023-11-09).
- (10) Bakhtiar, R. Surface Plasmon Resonance Spectroscopy: A Versatile Technique in a Biochemist's Toolbox. *J. Chem. Educ.* **2013**, *90* (2), 203–209. <https://doi.org/10.1021/ed200549g>.
- (11) Shankaran, D. R.; Gobi, K. V.; Miura, N. Recent Advancements in Surface Plasmon Resonance Immunosensors for Detection of Small Molecules of Biomedical, Food and Environmental Interest. *Sens. Actuators B Chem.* **2007**, *121* (1), 158–177. <https://doi.org/10.1016/j.snb.2006.09.014>.
- (12) Stockman, M. I. Nanoplasmonics: Past, Present, and Glimpse into Future. *Opt Express* **2011**, *19*. <https://doi.org/10.1364/OE.19.022029>.
- (13) Knight, M. W. Aluminum for Plasmonics. *ACS Nano* **2014**, *8*. <https://doi.org/10.1021/nn405495q>.
- (14) Liu, N.; Tang, M. L.; Hentschel, M.; Giessen, H.; Alivisatos, A. P. Nanoantenna-Enhanced Gas Sensing in a Single Tailored Nanofocus. *Nat Mater* **2011**, *10*. <https://doi.org/10.1038/nmat3029>.
- (15) Fedyanin, D. Y.; Yakubovsky, D. I.; Kirtaev, R. V.; Volkov, V. S. Ultralow-Loss CMOS Copper Plasmonic Waveguides. *Nano Lett* **2016**, *16*. <https://doi.org/10.1021/acs.nanolett.5b03942>.

- (16) Yang, Y. Ultraviolet–Visible Plasmonic Properties of Gallium Nanoparticles Investigated by Variable-Angle Spectroscopic and Mueller Matrix Ellipsometry. *ACS Photonics* **2014**, *1*. <https://doi.org/10.1021/ph500042v>.
- (17) McMahon, J. M.; Schatz, G. C.; Gray, S. K. Plasmonics in the Ultraviolet with the Poor Metals Al, Ga, In, Sn, Tl, Pb, and Bi. *Phys Chem Chem Phys* **2013**, *15*. <https://doi.org/10.1039/C3CP43856B>.
- (18) Wu, P. C. Real-Time Plasmon Resonance Tuning of Liquid Ga Nanoparticles by in Situ Spectroscopic Ellipsometry. *Appl Phys Lett* **2007**, *9*. <https://doi.org/10.1063/1.2712508>.
- (19) Zhang, T. Gallium Platinum Alloys - a New Material System for UV Plasmonics. *Opt Mater Express* **2017**, *7*. <https://doi.org/10.1364/OME.7.002880>.
- (20) Naik, G. V.; Shalaev, V. M.; Boltasseva, A. Alternative Plasmonic Materials: Beyond Gold and Silver. *Adv Mater* **2013**, *25*. <https://doi.org/10.1002/adma.201205076>.
- (21) Sanz, J. M. UV Plasmonic Behavior of Various Metal Nanoparticles in the Near- and Far-Field Regimes: Geometry and Substrate Effects. *J Phys Chem C* **2013**, *117*. <https://doi.org/10.1021/jp405773p>.
- (22) Appusamy, K.; Blair, S.; Nahata, A.; Guruswamy, S. Low-Loss Magnesium Films for Plasmonics. *Mater Sci Eng B* **2014**, *181*. <https://doi.org/10.1016/j.mseb.2013.11.009>.
- (23) Toudert, J.; Serna, R. Ultraviolet-Visible Interband Plasmonics with p-Block Elements. *Opt Mater Express* **2016**, *6*. <https://doi.org/10.1364/OME.6.002434>.
- (24) Cuadrado, A.; Toudert, J.; Serna, R. Polaritonic-to-Plasmonic Transition in Optically Resonant Bismuth Nanospheres for High-Contrast Switchable Ultraviolet Meta-Filters. *IEEE Photonics J* **2016**, *8*. <https://doi.org/10.1109/JPHOT.2016.2574777>.
- (25) Morales, D.; Stoute, N. A.; Yu, Z.; Aspnes, D. E.; Dickey, M. D. Liquid Gallium and the Eutectic Gallium Indium (EGaIn) Alloy: Dielectric Functions from 1.24 to 3.1 eV by Electrochemical Reduction of Surface Oxides. *Appl Phys Lett* **2016**, *109*. <https://doi.org/10.1063/1.4961910>.
- (26) Maksymov, I. S. Reviews in Physics Magneto-Plasmonic Nanoantennas: Basics and Applications. *Rev Phys* **2016**, *1*. <https://doi.org/10.1016/j.revip.2016.03.002>.
- (27) Lu, Y. Transformable Liquid-Metal Nanomedicine. *Nat Commun* **2015**, *6*.
- (28) Marín, A. G. Gallium Plasmonic Nanoparticles for Label-Free DNA and Single Nucleotide Polymorphism Sensing. *Nanoscale* **2016**, *8*. <https://doi.org/10.1039/C6NR00926C>.
- (29) Strobbia, P.; Cullum, B. M. Recent Advances in Plasmonic Nanostructures for Sensing: A Review. *SPIE Opt Eng* **2015**, *54*. <https://doi.org/10.1117/1.OE.54.10.100902>.
- (30) Fatakdwala, H. Fluorescence Lifetime Imaging Combined with Conventional Intravascular Ultrasound for Enhanced Assessment of Atherosclerotic Plaques: An Ex Vivo Study in Human Coronary Arteries. *J Cardiovasc Trans Res* **2015**, *8*. <https://doi.org/10.1007/s12265-015-9627-3>.
- (31) Bourantas, C. V. Hybrid Intravascular Imaging: Recent Advances, Technical Considerations, and Current Applications in the Study of Plaque Pathophysiology. *Eur Heart J* **2017**, *38*. <https://doi.org/10.1093/eurheartj/ehw097>.
- (32) Wang, B. Intravascular Photoacoustic Imaging. *IEEE J Quantum Electron* **2010**, *16*. <https://doi.org/10.1109/JSTQE.2009.2037023>.
- (33) Knight, M. W. Gallium Plasmonics: Deep Subwavelength Spectroscopic Imaging of Single and Interacting Gallium Nanoparticles. *ACS Nano* **2015**, *9*. <https://doi.org/10.1021/nn5072254>.

- (34) Lin, Y.; Liu, Y.; Genzer, J.; Dickey, M. D. Shape-Transformable Liquid Metal Nanoparticles in Aqueous Solution. *Chem Sci* **2017**, *8*. <https://doi.org/10.1039/C7SC00057J>.
- (35) Huang, Z.; Guan, M.; Bao, Z.; Dong, F.; Cui, X.; Liu, G. Ligand Mediation for Tunable and Oxide Suppressed Surface Gold-Decorated Liquid Metal Nanoparticles. *Small* **2024**, *20* (7), 2306652. <https://doi.org/10.1002/sml.202306652>.
- (36) Sun, W.; Nan, J.; Che, Y.; Shan, H.; Sun, Y.; Xu, W.; Zhu, S.; Zhang, J.; Yang, B. Liquid-Metal-Based Microfluidic Nanoplasmonic Platform for Point-of-Care Naked-Eye Antibody Detection. *Biosens. Bioelectron.* **2024**, *261*, 116469. <https://doi.org/10.1016/j.bios.2024.116469>.
- (37) *Stretchable and Soft Electronics using Liquid Metals - Dickey - 2017 - Advanced Materials - Wiley Online Library*. <https://onlinelibrary.wiley.com/doi/abs/10.1002/adma.201606425> (accessed 2023-11-09).
- (38) Tang, S.-Y.; Tabor, C.; Kalantar-Zadeh, K.; Dickey, M. D. Gallium Liquid Metal: The Devil's Elixir. *Annu. Rev. Mater. Res.* **2021**, *51* (1), 381–408. <https://doi.org/10.1146/annurev-matsci-080819-125403>.
- (39) Daeneke, T.; Khoshmanesh, K.; Mahmood, N.; Castro, I. A. de; Esrafilzadeh, D.; Barrow, S. J.; Dickey, M. D.; Kalantar-zadeh, K. Liquid Metals: Fundamentals and Applications in Chemistry. *Chem. Soc. Rev.* **2018**, *47* (11), 4073–4111. <https://doi.org/10.1039/C7CS00043J>.
- (40) *Liquid Metal-Based Soft Microfluidics - Zhu - 2020 - Small - Wiley Online Library*. <https://onlinelibrary.wiley.com/doi/abs/10.1002/sml.201903841> (accessed 2023-11-09).
- (41) Dickey, M. D. Emerging Applications of Liquid Metals Featuring Surface Oxides. *ACS Appl. Mater. Interfaces* **2014**, *6* (21), 18369–18379. <https://doi.org/10.1021/am5043017>.
- (42) Kalantar-Zadeh, K.; Tang, J.; Daeneke, T.; O'Mullane, A. P.; Stewart, L. A.; Liu, J.; Majidi, C.; Ruoff, R. S.; Weiss, P. S.; Dickey, M. D. Emergence of Liquid Metals in Nanotechnology. *ACS Nano* **2019**, *13* (7), 7388–7395. <https://doi.org/10.1021/acsnano.9b04843>.
- (43) *A Short History of Fusible Metals and Alloys – Towards Room Temperature Liquid Metals - Handschuh-Wang - 2022 - European Journal of Inorganic Chemistry - Wiley Online Library*. <https://chemistry-europe.onlinelibrary.wiley.com/doi/abs/10.1002/ejic.202200313> (accessed 2023-11-09).
- (44) Lin, Y.; Genzer, J.; Dickey, M. D. Attributes, Fabrication, and Applications of Gallium-Based Liquid Metal Particles. *Adv. Sci.* **2020**, *7* (12), 2000192. <https://doi.org/10.1002/advs.202000192>.
- (45) Babatatin, W.; Kim, M. S.; Hussain, M. M. From Droplets to Devices: Recent Advances in Liquid Metal Droplet Enabled Electronics. *Adv. Funct. Mater.* *n/a* (n/a), 2308116. <https://doi.org/10.1002/adfm.202308116>.
- (46) Jamalzadegan, S.; Kim, S.; Mohammad, N.; Koduri, H.; Hetzler, Z.; Lee, G.; Dickey, M. D.; Wei, Q. Liquid Metal-Based Biosensors: Fundamentals and Applications. *Adv. Funct. Mater.* *n/a* (n/a), 2308173. <https://doi.org/10.1002/adfm.202308173>.
- (47) *Band structure and optical properties of gallium - IOPscience*. <https://iopscience.iop.org/article/10.1088/0305-4608/4/11/032/meta> (accessed 2023-11-09).
- (48) Bhardwaj, A.; Verma, S. S. Simulations of Optical Properties of Gallium Alloy Nanorods Based on Aspect Ratio and Shell Thickness. *Mater. Today Commun.* **2023**, *37*, 107135. <https://doi.org/10.1016/j.mtcomm.2023.107135>.
- (49) Bhardwaj, A.; Bhatia, P.; Verma, S. S. Plasmonic Properties of Silver Coated Non-Spherical Gallium Alloy Nanoparticles. *Opt. Quantum Electron.* **2022**, *55* (1), 40. <https://doi.org/10.1007/s11082-022-04321-3>.

- (50) Bhardwaj, A.; Verma, S. S. Theoretical Study on Plasmonic Applications of Gallium Alloy (GaX, X = Ag, Al, Hg and In) Nanospheres and Nanoshells. *J. Quant. Spectrosc. Radiat. Transf.* **2022**, *281*, 108109. <https://doi.org/10.1016/j.jqsrt.2022.108109>.
- (51) Reineck, P.; Lin, Y.; Gibson, B. C.; Dickey, M. D.; Greentree, A. D.; Maksymov, I. S. UV Plasmonic Properties of Colloidal Liquid-Metal Eutectic Gallium-Indium Alloy Nanoparticles. *Sci. Rep.* **2019**, *9* (1), 5345. <https://doi.org/10.1038/s41598-019-41789-8>.
- (52) Ma, J.; Krisnadi, F.; Vong, M. H.; Kong, M.; Awartani, O. M.; Dickey, M. D. Shaping a Soft Future: Patterning Liquid Metals. *Adv. Mater.* *n/a* (n/a), 2205196. <https://doi.org/10.1002/adma.202205196>.
- (53) Liu, P. Q.; Miao, X.; Datta, S. Recent Advances in Liquid Metal Photonics: Technologies and Applications [Invited]. *Opt. Mater. Express* **2023**, *13* (3), 699–727. <https://doi.org/10.1364/OME.484236>.
- (54) Yu, Z. Discovery of a Voltage-Stimulated Heartbeat Effect in Droplets of Liquid Gallium. *Phys Rev Lett* **2018**, *121*. <https://doi.org/10.1103/PhysRevLett.121.024302>.
- (55) Lear, T. R. Liquid Metal Particle Popping: Macroscale to Nanoscale. *Extrem Mech Lett* **2017**, *13*. <https://doi.org/10.1016/j.eml.2017.02.009>.
- (56) Connor, S. Introduction to the Finite-Difference Time-Domain (FDTD) Technique. **2008**. <https://doi.org/10.1109/ISEMC.2008.4652175>.
- (57) Fu, Q.; Sun, W. Mie Theory for Light Scattering by a Spherical Particle in an Absorbing Medium. *Appl. Opt.* **2001**, *40* (9), 1354–1361. <https://doi.org/10.1364/AO.40.001354>.
- (58) Joshipura, I. D.; Nguyen, C. K.; Quinn, C.; Yang, J.; Morales, D. H.; Santiso, E.; Daeneke, T.; Truong, V. K.; Dickey, M. D. An Atomically Smooth Container: Can the Native Oxide Promote Supercooling of Liquid Gallium? *iScience* **2023**, *26* (4), 106493. <https://doi.org/10.1016/j.isci.2023.106493>.
- (59) Li, Z.; Zhang, H.; Wang, D.; Gao, C.; Sun, M.; Wu, Z.; He, Q. Reconfigurable Assembly of Active Liquid Metal Colloidal Cluster. *Angew. Chem. Int. Ed.* **2020**, *59* (45), 19884–19888. <https://doi.org/10.1002/anie.202007911>.
- (60) Ikuno, T.; Somei, Z. Fabrication of Eutectic Ga-In Nanowire Arrays Based on Plateau–Rayleigh Instability. *Molecules* **2021**, *26* (15), 4616. <https://doi.org/10.3390/molecules26154616>.
- (61) Huang, C.-C.; Yeh, C.-S.; Ho, C.-J. Laser Ablation Synthesis of Spindle-like Gallium Oxide Hydroxide Nanoparticles with the Presence of Cationic Cetyltrimethylammonium Bromide. *J. Phys. Chem. B* **2004**, *108* (16), 4940–4945. <https://doi.org/10.1021/jp037427n>.
- (62) Yoon, J. H.; Selbach, F.; Schumacher, L.; Jose, J.; Schlücker, S. Surface Plasmon Coupling in Dimers of Gold Nanoparticles: Experiment and Theory for Ideal (Spherical) and Nonideal (Faceted) Building Blocks. *ACS Photonics* **2019**, *6* (3), 642–648. <https://doi.org/10.1021/acsp Photonics.8b01424>.
- (63) Hao, E.; Schatz, G. C. Electromagnetic Fields around Silver Nanoparticles and Dimers. *J. Chem. Phys.* **2003**, *120* (1), 357–366. <https://doi.org/10.1063/1.1629280>.
- (64) Yan, J.; Malakooti, M. H.; Lu, Z.; Wang, Z.; Kazem, N.; Pan, C.; Bockstaller, M. R.; Majidi, C.; Matyjaszewski, K. Solution Processable Liquid Metal Nanodroplets by Surface-Initiated Atom Transfer Radical Polymerization. *Nat. Nanotechnol.* **2019**, *14* (7), 684–690. <https://doi.org/10.1038/s41565-019-0454-6>.
- (65) Khan, M. A. K.; Zhao, Y.; Datta, S.; Paul, P.; Vasini, S.; Thundat, T.; Liu, P. Q. Deterministic Fabrication of Liquid Metal Nanopatterns for Nanophotonics Applications. *Small* *n/a* (n/a), 2403722. <https://doi.org/10.1002/smll.202403722>.

- (66) Hetzler, Z.; Wang, Y.; Krafft, D.; Jamalzadegan, S.; Overton, L.; Kudenov, M. W.; Ligler, F. S.; Wei, Q. Flexible Sensor Patch for Continuous Carbon Dioxide Monitoring. *Front. Chem.* **2022**, *10*.
- (67) Lee, G.; Hossain, O.; Jamalzadegan, S.; Liu, Y.; Wang, H.; Saville, A. C.; Shymanovich, T.; Paul, R.; Rotenberg, D.; Whitfield, A. E.; Ristaino, J. B.; Zhu, Y.; Wei, Q. Abaxial Leaf Surface-Mounted Multimodal Wearable Sensor for Continuous Plant Physiology Monitoring. *Sci. Adv.* **2023**, *9* (15), eade2232. <https://doi.org/10.1126/sciadv.ade2232>.

Supplementary Information

Shape and Size-Dependent Surface Plasmonic Resonances of Liquid Metal Alloy (EGaIn) Nanoparticles

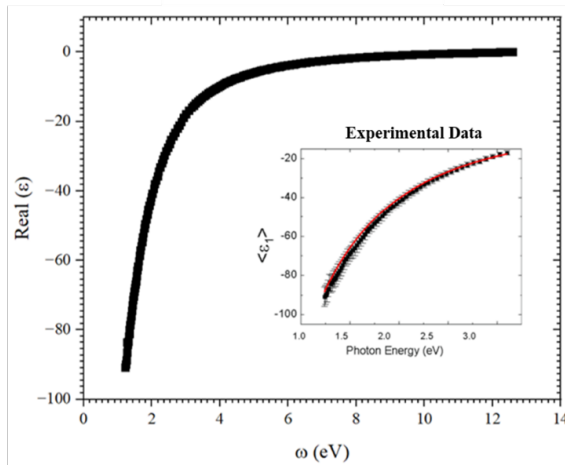
Sina Jamalzadegan¹, Alireza Velayati¹, Mohammadreza Zare¹, Michael D. Dickey^{1}, and Qingshan Wei^{1*}*

¹Department of Chemical and Biomolecular Engineering, North Carolina State University, Raleigh, NC 27695, USA

* Co-corresponding: qwei3@ncsu.edu and mddickey@ncsu.edu

(a)

$$\varepsilon_1(E) = 1 - \frac{E_p^2}{(E^2 + \gamma^2)}$$



(b)

$$\varepsilon_2(E) = \frac{E_p^2 \gamma}{E(E^2 + \gamma^2)}$$

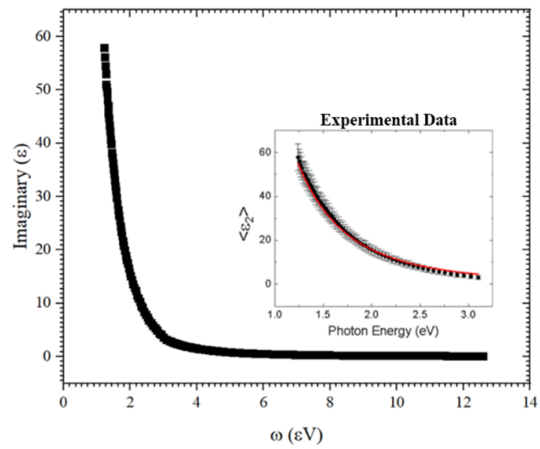
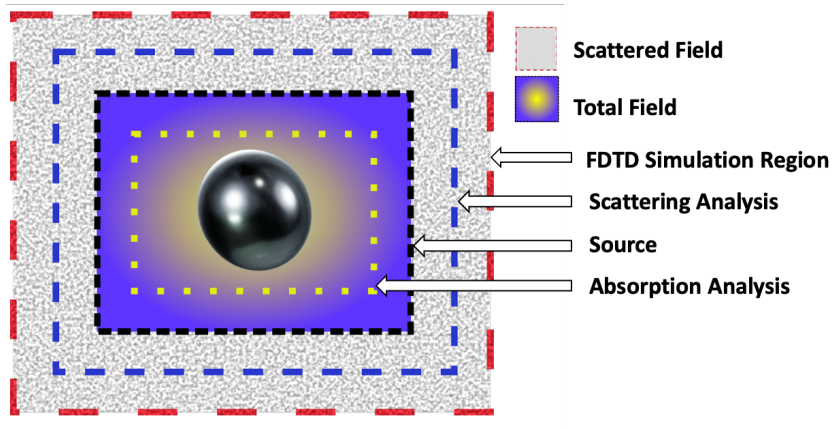


Figure S1. Extrapolated and experimental¹ values (insets) for a) the real part and b) the imaginary part of the permittivity of EGaIn in the 100–1000 nm wavelength range.

(a)



(b)

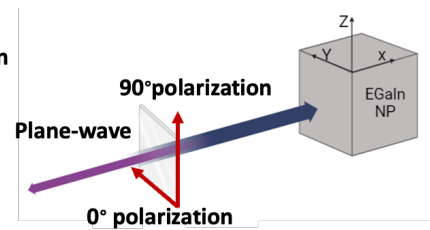


Figure S2. a) Schematic of FDTD simulation Setup, b) Schematic of the incidence light source and polarization angle.

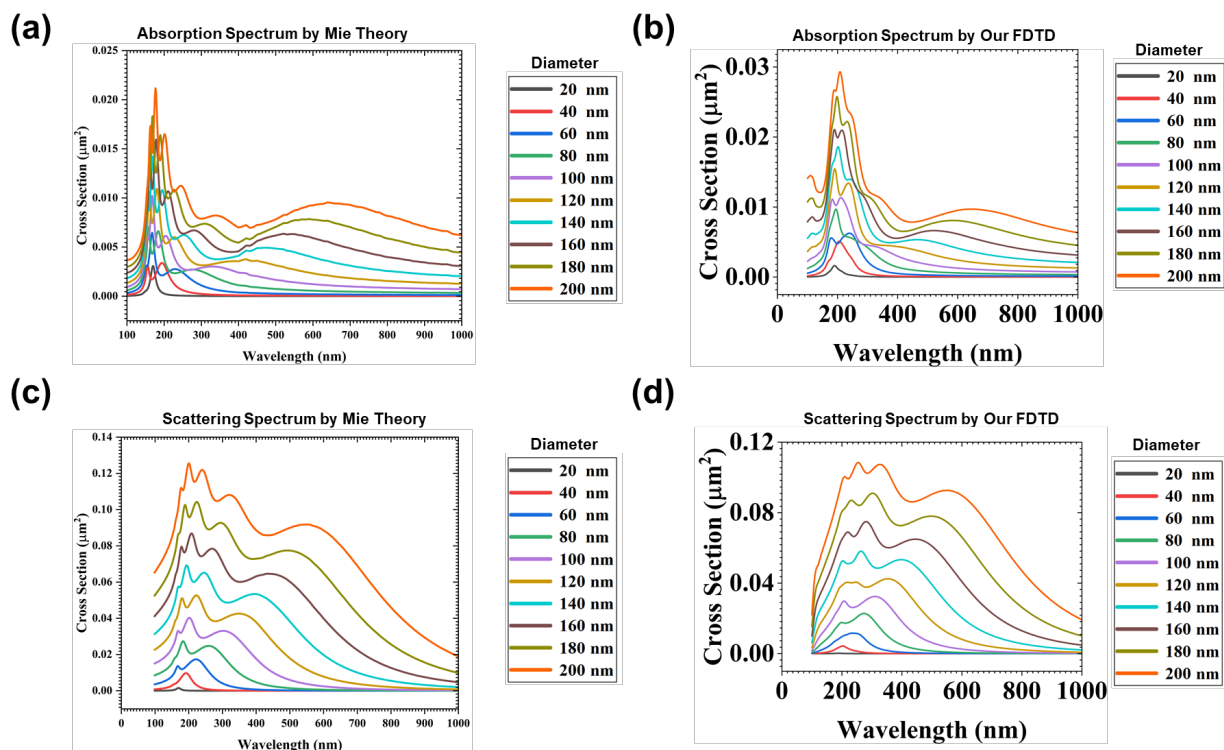
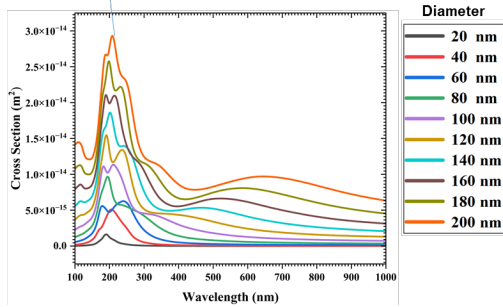
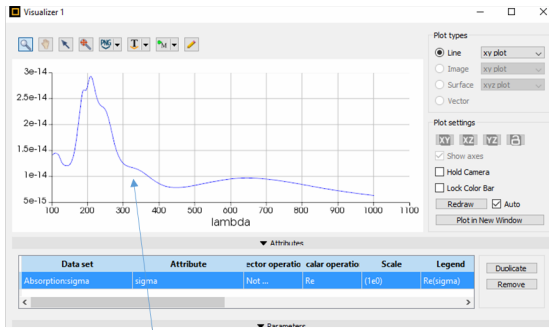


Figure S3. Absorption spectra of various diameters of single EGaIn spherical nanoparticles by applying a) Mie theory and b) FDTD simulation. Scattering spectra of various diameters of single EGaIn spherical nanoparticles by applying c) Mie theory and d) FDTD simulation.

Absorption spectrum of 200 nm diameter single EGaIn nanoparticle with 6 nm oxide layer



Scattering spectrum of 200 nm diameter single EGaIn nanoparticle with 6 nm oxide layer

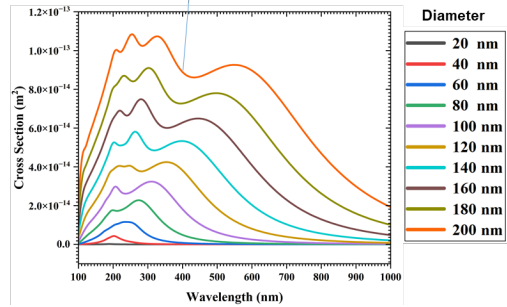
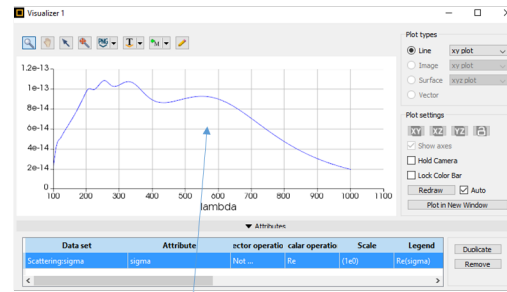


Figure S4. The absorption and scattering spectra of a single spherical EGaIn nanoparticle with a 200 nm diameter and a 6 nm oxide layer show no changes compared to a single spherical EGaIn nanoparticle without an oxide layer.

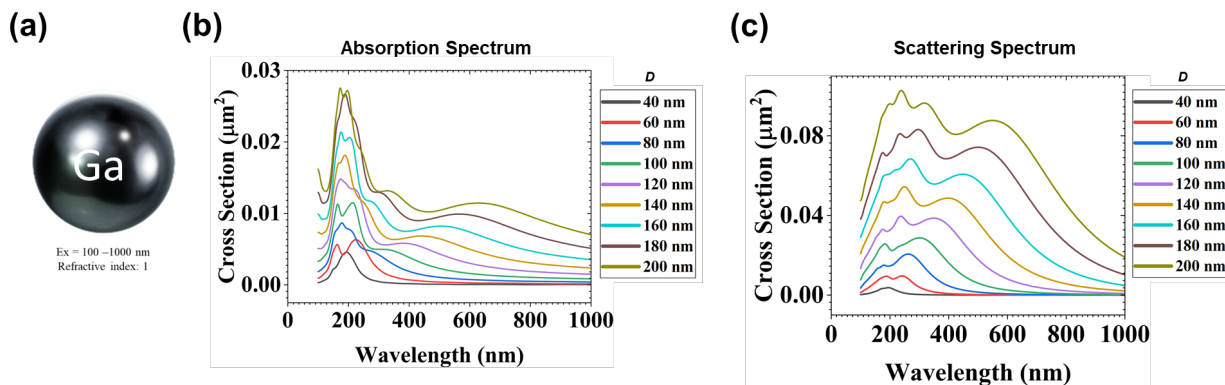


Figure S5. a) 3D schematic of a single spherical Ga nanoparticle. FDTD simulation results of b) absorption and c) scattering spectra of various diameters of single Ga spherical nanoparticles. Ga nanosphere is excited by a plane-wave source of 100-1000 nm wavelength in the x-direction with a polarized angle of 90 degree.

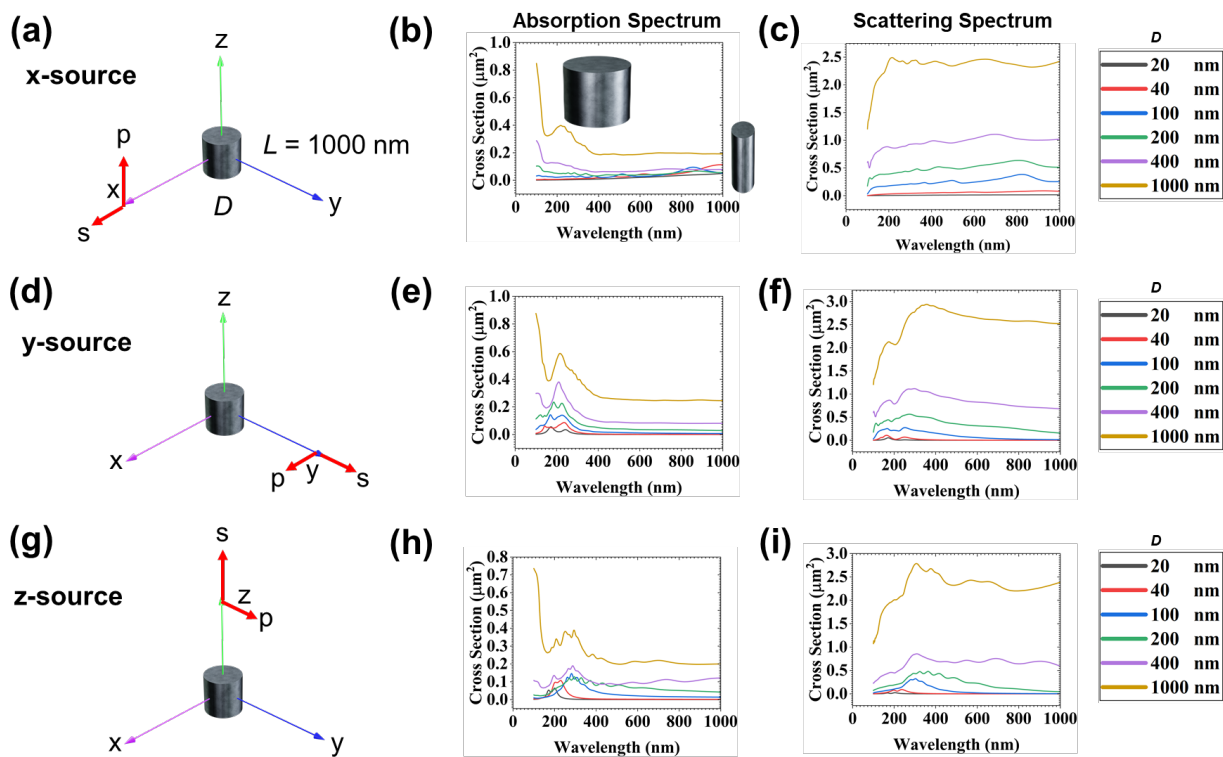


Figure S6. Plasmonic resonance behavior of single EGaIn nanorod with tunable diameters.

a,d,g) 3D schematic of single EGaIn nanorod excited by a plane-wave light source (s) in x-, y-, and z-direction with 90 degree polarization (p), respectively. b,e,h) Absorption and c,f,i) scattering cross section spectra for various diameters with a constant length of 1000 nm.

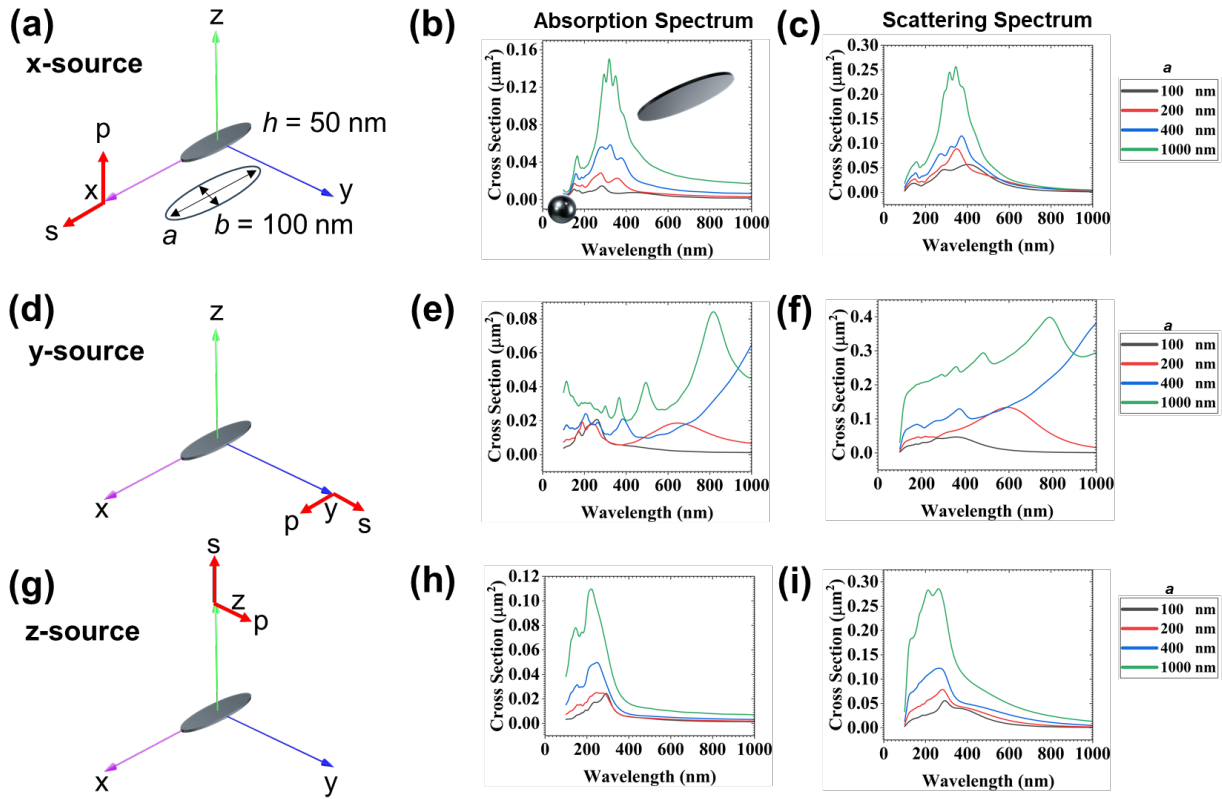


Figure S7. Plasmonic resonance behavior of single EGaIn nanoellipse. a,d,g) 3D schematic of single EGaIn nanoellipse excited by a plane-wave light source (s) in x -, y -, and z -directions with 90 degree polarization (p), respectively. b,e,h) Absorption and c,f,i) scattering cross section spectra for nanoellipses with a constant thickness of 50 nm and minor axis of 100 nm.

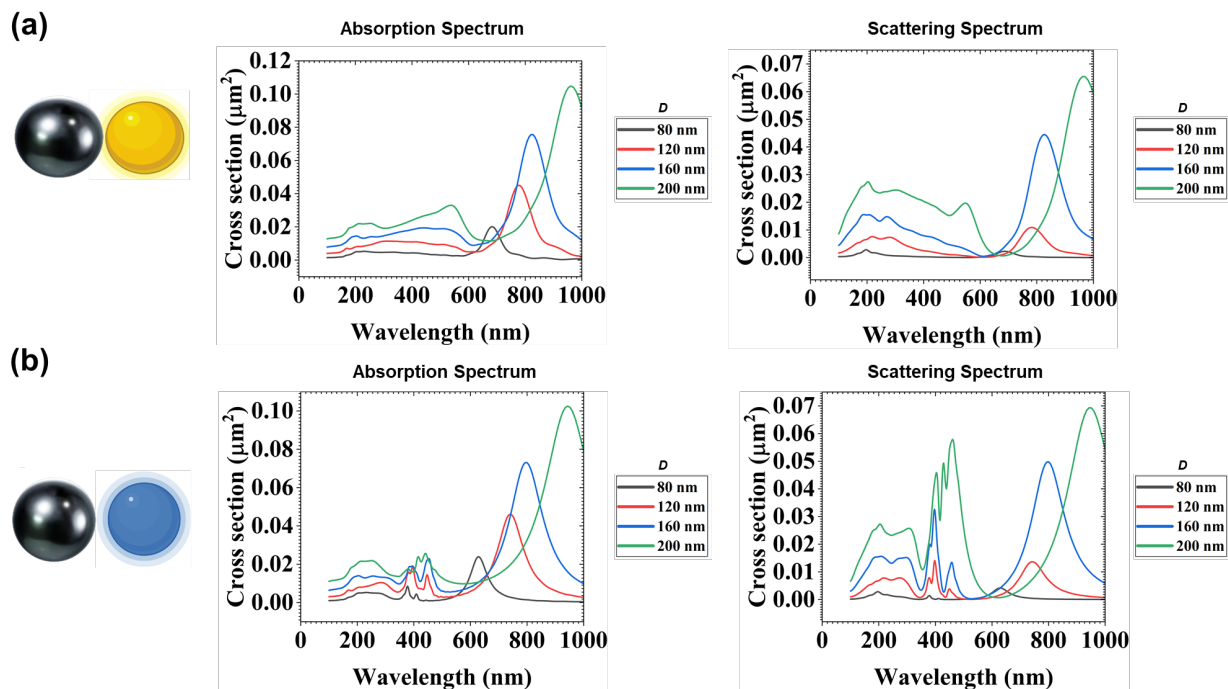


Figure S8. a) Absorption and b) scattering spectrum of various radius of dimer EGaIn-Au spherical nanoparticles and also c) Absorption and d) scattering spectrum various radius of dimer EGaIn-Ag spherical applying FDTD simulation by using plane-wave source with 100-1000 nm wavelength in x-direction with polarized angle 90 degree.

References

- 1) Morales, D.; Stoute, N. A.; Yu, Z.; Aspnes, D. E.; Dickey, M. D. Liquid Gallium and the Eutectic Gallium Indium (EGaIn) Alloy: Dielectric Functions from 1.24 to 3.1 eV by Electrochemical Reduction of Surface Oxides. *Appl Phys Lett* **2016**, *109*. <https://doi.org/10.1063/1.4961910>.